

Occam Learning

Rongrong Xie

Key Laboratory of Quark and Lepton Physics (MOE) and Institute of Particle Physics,
Central China Normal University (CCNU), Wuhan, China

and

Matteo Marsili*

Quantitative Life Sciences Section

The Abdus Salam International Centre for Theoretical Physics, 34151 Trieste, Italy

Abstract

We discuss probabilistic neural network models for unsupervised learning where the distribution of the hidden layer is fixed. We argue that learning machines with this architecture enjoy a number of desirable properties. For example, the model can be chosen as a simple and interpretable one, it does not need to be over-parametrised and training is argued to be efficient in a thermodynamic sense.

When hidden units are binary variables, these models have a natural interpretation in terms of features. We show that the featureless state corresponds to a state of maximal ignorance about the features and that learning the first feature depends on non-Gaussian statistical properties of the data. We suggest that the distribution of hidden variables should be chosen according to the principle of maximal relevance. We introduce the Hierarchical Feature Model (HFM) as an example of a model that satisfies this principle, and that encodes a neutral *a priori* organisation of the feature space.

We present extensive numerical experiments in order *i)* to test that the internal representation of learning machines can indeed be independent of the data with which they are trained and *ii)* that only a finite number of features are needed to describe a number of datasets.

Frustra fit per plura quod fieri potest per pauciora

(William of Ockham)

The Occam razor prescribes that, among competing explanations of the same phenomenon, the simplest should be chosen. The rationale for Occam razor in statistical learning is that, if the model is a compressed representation of the data, the simpler the

*marsili@ictp.it

model, the more we learn¹. Very complex models may reproduce accurately the data, but they fail to generalise well, i.e. to describe yet unseen data-points in a satisfactory manner – a phenomenon called overfitting.

Recent advances in machine learning challenge this view, showing that accuracy in deep neural networks can increase with complexity (i.e. with the number of parameters), without overfitting [1]. In spite of spectacular advances in tasks such as automatic translation, image classification and speech recognition, the reasons why such over-parametrized models work so well is yet not well understood (yet see [2]), and recipes for designing architectures, at the time of writing, are mostly driven by trial and error.

This work attempts to vindicate Occam razor, showing that in the case of unsupervised learning within probabilistic single layer neural networks, it is possible to have a first principle approach to statistical learning consistent with Occam razor. Our approach builds on previous work [3] that suggests that in all learned models, a complex dataset is associated to an internal representation² of maximal relevance (see later). This, in turn, suggests to explore model architectures where the internal representation is fixed *a priori* as a probability distribution of maximal relevance, and only the conditional distribution of the data, given the internal state, is learned. We argue that this approach has several advantages with respect to traditional ones – such as Restricted Boltzmann Machines (RBM) – in terms of conceptual clarity, parsimony of internal variables and energetic costs of training. In addition it enables functions that go beyond the mere learning and generalisation paradigm of machine learning.

The rest of the paper is organised as follows: Section 1 sets the stage by defining precisely the framework that we shall deal with throughout the paper. Taking RBMs as a paradigmatic example, Section 1 also discusses critical issues in their use. Section 2 discusses architectures where the internal representation is fixed. It also introduces the Hierarchical Feature Model (HFM) as a special example of an internal representation which conforms with the principle of maximal relevance. Section 3 then presents the results of numerical experiments of training machines with a fixed internal representation on a variety of datasets. We conclude with a Section that summarises the results and discusses their relation to other problems in machine learning and on possible extensions.

1 Single layer probabilistic neural networks

We focus on unsupervised learning and, in particular, on probabilistic single layer neural networks composed by a vector of m binary variables $\mathbf{x} = (x_1, \dots, x_m)$ coupled to a vector $\mathbf{s} = (s_1, \dots, s_n)$ of n binary variables ($x_j, s_i \in \{0, 1\}$). \mathbf{x} is called the visible layer whereas \mathbf{s} is the hidden layer. The network is defined by a joint probability distribution $p(\mathbf{x}, \mathbf{s}|\theta)$

¹In this paper we're going to assume that a simple model is one that depends on few parameters.

²The internal representation of a learning machine is the unconditional probability distribution of its internal states (see Eq. 5).

over the visible and the hidden variables, that depends on a vector θ of parameters.

For example, in a Restricted Boltzmann Machine (RBM) the joint probability distribution is given by

$$p(\mathbf{x}, \mathbf{s}|\theta) = \frac{1}{Z(\theta)} e^{-E(\mathbf{x}, \mathbf{s}|\theta)} \quad (1)$$

where Z is a normalisation constant and the "energy" function

$$E(\mathbf{x}, \mathbf{s}|\theta) = \sum_{j=1}^m b_j x_j + \sum_{i=1}^n c_i s_i + \sum_{i,j} s_i u_{i,j} x_j \quad (2)$$

depends on the parameters $\theta = \{b_j, c_i, u_{i,j}, i = 1, \dots, n; j = 1, \dots, m\}$.

Given a dataset $\hat{\mathbf{x}} = (\mathbf{x}^{(1)}, \dots, \mathbf{x}^{(N)})$ of N samples of the visible variables, the network is trained by maximising the log-likelihood

$$\mathcal{L}(\hat{\mathbf{x}}|\theta) = \sum_{i=1}^N \log p(\mathbf{x}^{(i)}|\theta), \quad (3)$$

over θ , where

$$p(\mathbf{x}|\theta) = \sum_{\mathbf{s}} p(\mathbf{x}, \mathbf{s}|\theta) \quad (4)$$

is the marginal distribution of \mathbf{x} . We'll denote by $\hat{\theta} = \arg \max_{\theta} \mathcal{L}(\hat{\mathbf{x}}|\theta)$ the learned parameters (after training). Training maps the dataset $\hat{\mathbf{x}}$ onto an internal representation

$$p(\mathbf{s}|\hat{\theta}) = \sum_{\mathbf{x}} p(\mathbf{x}, \mathbf{s}|\hat{\theta}) \quad (5)$$

which is the marginal distribution over hidden states \mathbf{s} .

In a learning machine such as a RBM, the joint distribution $p(\mathbf{x}, \mathbf{s}|\theta)$ is defined so that the variables \mathbf{x} and \mathbf{s} are easy to sample by Montecarlo Markov chain methods. This allows one to estimate the gradients of the log-likelihood. During training both the internal representation $p(\mathbf{s}|\theta)$ and the conditional distribution $p(\mathbf{x}|\mathbf{s}, \theta)$ are learned from scratch.

In practice, efficient training protocols need to resort to few expedients, such as:

stochastic gradient ascent: in order to avoid local maxima, the gradients of the likelihood are estimated on a random subset of data points (mini-batches).

over-parametrisation: in order to make the log-likelihood landscape flat enough, the number of parameters needs to be large, typically of the same order or larger than the number of data points.

random initial conditions the log-likelihood landscape is highly degenerate³. This degeneracy is broken by starting training from a random point θ_0 .

This paper explores architectures

$$p(\mathbf{x}, \mathbf{s}|\theta) = p(\mathbf{x}|\mathbf{s}, \theta)p(\mathbf{s}) \quad (6)$$

where the internal representation $p(\mathbf{s})$ is fixed at the outset, and only the conditional distribution $p(\mathbf{x}|\mathbf{s}, \theta)$ is learned. There are two key questions that one should address:

- 1) how to choose a “good” $p(\mathbf{s})$?
- 2) does any “good” $p(\mathbf{s})$ works equally well for any dataset?

We draw from [4, 3] to answer the first question. There it is argued that the internal representation of learning machines trained on a dataset with a rich structure should obey a principle of maximal relevance. We refer to Ref. [3] for a detailed discussion. Let it suffice to say that the relevance is the entropy of the distribution of coding costs $E_{\mathbf{s}} \equiv -\log p(\mathbf{s})$. So a distribution of maximal relevance is characterised by a distribution of $E_{\mathbf{s}}$ which is as broad as possible, consistent with a given average coding cost

$$\mathbb{E}[E_{\mathbf{s}}] = -\sum_{\mathbf{s}} p(\mathbf{s}) \log p(\mathbf{s}) \equiv H[\mathbf{s}]. \quad (7)$$

$H[\mathbf{s}]$ quantifies the compression level and is henceforth called resolution, following Ref. [3]. Refs. [4, 5] show that RBM, Deep Belief Networks and other architectures satisfy this principle reasonably well. The principle of maximal relevance then provides a guide on how the distribution $p(\mathbf{s})$ in Eq. (6) should be chosen. In particular, this principle dictates that the number $W(E)$ of states \mathbf{s} with coding cost $-\log p(\mathbf{s}) = E$ should follow an exponential law, $W(E) = W_0 e^{cE}$.

As for the second question, architectures where the internal representation is fixed at the outset and only the output layer is learned have been proposed for supervised learning tasks (see e.g. [6, 7, 8]). Their success suggests that the internal representation may be largely independent of the data being learned. In Section 3.1 we will provide further evidence in unsupervised learning, showing that a representation $p(\mathbf{s})$ learned from a dataset can be used in architectures with a fixed $p(\mathbf{s})$ to learn a different dataset. This corroborates the hypothesis that $p(\mathbf{s})$ can indeed be independent of the training data.

There are several reasons why an approach to learning with a fixed $p(\mathbf{s})$ is conceptually preferable:

³In RBM, any transformation $\mathbf{s} \rightarrow \mathbf{s}'$ that is accompanied by a “gauge” transformation $c_i \rightarrow c'_i = s_i s'_i c_i$, $u_{i,j} \rightarrow u'_{i,j} = s_i s'_i u_{i,j}$ leaves the likelihood invariant. Training by gradient ascent cannot start from the state $b_j = c_i = u_{i,j} = 0$ for all i and j because the only gradient which is non-zero is the one with respect to b_j . As long as $u_{i,j} = 0$, the data \mathbf{x} and the internal state \mathbf{s} remain independent, i.e. $p(\mathbf{x}, \mathbf{s}|\theta) = p(\mathbf{x}|\mathbf{b})2^{-n}$. Gradient ascent drives b_j to the point where the expected value of x_j over $p(\mathbf{x}|\mathbf{b})$ matches the empirical average, with derivatives with respect to c_i and $u_{i,j}$ that remain zero. This is why training needs to start from a random point θ_0 .

- As discussed in [9], the practical implementation of training algorithms (number of hidden nodes, of mini-batches, etc) relies on rules of thumb, which are often the result of a long trial and error process in the search of what works.
- The different hidden variables s_i in an RBM are all a priori equivalent. Some of the associated features $\vec{u}_i = (u_{i,1}, \dots, u_{i,m})$ converge to localised fields for highly structured datasets [10], but there is no hierarchical organisation of relevance among them. Fernandez *et al.* [11] observe that relevant information (e.g. on the labels of a dataset) is distributed on all hidden nodes of a RBM. The numerical experiments discussed below suggest that when a hierarchy between features is imposed by the choice of $p(\mathbf{s})$, relevant information on (e.g. on labels) concentrates on the top features.
- The representation with n features is in principle very different from the one learned with $n' > n$ features. So the phase space of a RBM cannot be expanded continuously in the training process. Choosing the $p(\mathbf{s})$ at the outset will allow us to give a precise organisation to the feature space and, as we shall see, add new features – if needed – without affecting already learned ones.
- The learned internal representation $p(\mathbf{s}|\hat{\theta})$ in a RBM is not unique, but it rather belongs to a manifold of possible distributions. The representation $p(\mathbf{s}|\hat{\theta})$ learned starting from two different initial conditions for the same dataset may be completely different. Because of the stochastic nature of the training process, upon adding further data points to the dataset (i.e. $N \rightarrow N' > N$) the learned representation may change completely. It is not clear how useful information on the structure of statistical dependencies of the data can be “read” from the learned model and how it can be disentangled from the effects of randomness in initial conditions and in the training process. As we shall see, a fixed $p(\mathbf{s})$ allows learning to follow a unique deterministic trajectory.
- There is no clear prescription on how to choose the number n of hidden variables for a given dataset in a RBM. In particular, the final compression level $H[\mathbf{s}]$ (or *resolution*) of the internal representation is a complicated function of n and of the data $\hat{\mathbf{x}}$. There is no recipe, besides trial and error, on the number of hidden units that should be taken in order to achieve a given compression level. Also there is no relation between representations at nearby compression levels, since they are the result of different training processes that may end up anywhere on the respective manifolds of distributions. Learning with a fixed $p(\mathbf{s})$ allows one to specify the resolution $H[\mathbf{s}]$ at the outset. Also, the resolution $H[\mathbf{s}]$ can be changed continuously by changing $p(\mathbf{s})$ and we expect the parameters θ of $p(\mathbf{x}|\mathbf{s}, \theta)$ to change continuously.
- Learning in RBMs typically starts at high temperatures – i.e. from a random state with weak interactions – and the machine “cools down” as weights and biases θ

increase⁴. In a scheme where $p(\mathbf{s})$ can be controlled, learning can start from low temperatures, i.e. from the ground state $\mathbf{s}_0 = \arg \max_{\mathbf{s}} p(\mathbf{s})$. In this first step, the model reproduces the global properties of the data, taking all the data point as elements of the same class. Next, as $p(\mathbf{s})$ broadens the model incorporates more and more details of the data, data points will differentiate into finer and finer classes. This way of learning starts from zero temperature and maximal compression ($H[\mathbf{s}] = 0$) and it expands $p(\mathbf{s})$ progressively.

- It has been recently pointed out [13] that the MCMC sampling used in RBMs to estimate likelihood gradients hardly reaches the equilibrium distribution. Sampling from the equilibrium distribution is trivial when $p(\mathbf{s})$ is chosen *a priori*.
- The training process is expected to be thermodynamically efficient when $p(\mathbf{s})$ is chosen appropriately. In order to see this, consider the following thermodynamic description of the training process: Initially, the data \mathbf{x} and the internal representation \mathbf{s} are independent random variables, i.e. the initial distribution is given by $p_0(\mathbf{x})p_0(\mathbf{s})$ where $p_0(\mathbf{x})$ is the (unknown) data distribution and $p_0(\mathbf{s}) = \sum_{\mathbf{x}} p(\mathbf{x}, \mathbf{s}|\theta_0)$ is the marginal distribution of the internal state of the machine. Training involves putting the two systems (the data and the machine) into contact, at a fixed temperature, and adjusting the weights of the machine until the data and the machine converge to a state $p_\infty(\mathbf{x}, \mathbf{s}) = p(\mathbf{x}, \mathbf{s}|\hat{\theta})$, which is such that the final marginal distribution of \mathbf{x} approximates the data distribution well, i.e. $p_\infty(\mathbf{x}) \approx p_0(\mathbf{x})$. Treating p_0 as an equilibrium distribution and learning as a process leading to a non-equilibrium state p_∞ , the minimal work done on the system in the process can be estimated as the non-equilibrium free energy[14] (see Appendix)

$$W \geq \Delta F \approx k_B T [I(\mathbf{x}, \mathbf{s}) + D_{KL}(p_\infty(\mathbf{s})||p_0(\mathbf{s}))], \quad (8)$$

where $I(\mathbf{x}, \mathbf{s})$ is the mutual information between the data and the internal state⁵ and the last term is the Kullback-Leibler divergence between the final and the initial distribution of \mathbf{s} . A thermodynamically optimal design of a learning machine is one where the final distribution $p_\infty(\mathbf{s})$ is as close as possible to the initial one. This is not the case for RBMs [4].

- There are several advantages in learning schemes where $p(\mathbf{s})$ is fixed. These architectures allow for tasks that go beyond reproducing data or generalising. For example,

⁴This is revealed by the fact that the distribution of energies $E_{\mathbf{s}} = -\log p(\mathbf{s}|\theta)$ is initially sharply peaked and the resolution, which is akin to the average energy in a physical model (see Eq. 7), is initially as large as possible, as shown in Ref. [4]. As training proceeds, the distribution of energies gets broader while the resolution $H[\mathbf{s}]$ follows a complex schedule of compressions and expansions [4, 12].

⁵We remind that $I(\mathbf{x}, \mathbf{s}) = H[\mathbf{s}] - H[\mathbf{s}|\mathbf{x}] \approx H[\mathbf{s}]$ in representations where \mathbf{s} is essentially a function of \mathbf{x} (i.e. $H[\mathbf{s}|\mathbf{x}] \approx 0$). This means that the first term in Eq. (8) is in practice the compression level $H[\mathbf{s}]$ of the internal representation.

once the conditional distributions $p(\mathbf{x}|\mathbf{s}, \hat{\theta})$ and $p(\mathbf{z}|\mathbf{s}, \hat{\theta}')$ are learned from two different datasets $\hat{\mathbf{x}}$ and $\hat{\mathbf{z}}$, it is possible to compute a joint distribution

$$p(\mathbf{x}, \mathbf{z}) = \sum_{\mathbf{s}} p(\mathbf{x}|\mathbf{s}, \hat{\theta})p(\mathbf{z}|\mathbf{s}, \hat{\theta}')p(\mathbf{s}) \quad (9)$$

that may shed light on possible relations between \mathbf{x} and \mathbf{z} . Drawing such hypothetical relations is a key aspect of intelligent behaviour. We shall also argue that architectures with a fixed $p(\mathbf{s})$ can generate combination of the learned features which are not observed in the data, an ability akin to imagination [15].

2 Occam learning machines

Let us now consider the problem of training a model of the type of Eq. (6). The log-likelihood can be written as

$$\mathcal{L} = \frac{1}{N} \log p(\hat{\mathbf{x}}|\theta) = \overline{\log p(\mathbf{x}|\theta)} = \overline{\log \mathbb{E}_{\mathbf{s}} [p(\mathbf{x}|\mathbf{s}, \theta)]} \quad (10)$$

where $\overline{g(\mathbf{x})} = \frac{1}{N} \sum_a g(\mathbf{x}^{(a)})$ denotes the average over the data of a generic function $g(\mathbf{x})$, and $\mathbb{E}_{\mathbf{s}}[\dots]$ stands for the expected value over $p(\mathbf{s})$. We assume that all statistical dependencies between the x_j are “explained” by the variable \mathbf{s} . This implies that, conditional on \mathbf{s} , all components of \mathbf{x} are independent, i.e.

$$p(\mathbf{x}|\mathbf{s}, \theta) = \prod_{j=1}^m \frac{e^{h_j(\mathbf{s})x_j}}{1 + e^{h_j(\mathbf{s})}}, \quad h_j(\mathbf{s}) = a_j + \sum_{i=1}^n s_i w_{i,j}. \quad (11)$$

We shall interpret the vector $\vec{w}_i = (w_{i,1}, \dots, w_{i,m})$ as *feature i* . Hence points \mathbf{x} drawn from $p(\mathbf{x}|\mathbf{s}, \theta)$ with $s_i = 1$ are characterised by feature i , whereas if $s_i = 0$ the distribution $p(\mathbf{x}|\mathbf{s}, \theta)$ generates points without feature i . The internal configuration \mathbf{s} then specifies a profile of features.

The distribution $p(\mathbf{s})$ instead encodes the way in which the space of features is populated.

2.1 The featureless state

Let us consider the *featureless state* $p(\mathbf{s}) = \delta_{\mathbf{s}, \mathbf{s}_0}$ where $\mathbf{s}_0 = (0, 0, \dots, 0)$ is the state where $s_i = 0$ for all $i = 1, \dots, n$. This state corresponds to zero coding cost, i.e. $H[\mathbf{s}] = 0$ and it is akin to a zero temperature state.

The probability $p(\mathbf{x}|\mathbf{s}, \theta)$ then depends only on the parameters a_j , and the likelihood is maximal when

$$a_j = \log \frac{\bar{x}_j}{1 - \bar{x}_j}, \quad \forall j. \quad (12)$$

In this state, the data does not provide any information on the features. With a flat prior on \vec{w}_i the posterior remains a flat, totally uninformative distribution⁶. It is conceptually appealing that the featureless state corresponds to a state of maximal ignorance about the features.

2.2 Learning one feature at a time

With increasing resolution $H[\mathbf{s}]$ we're led to study distributions where $p(\mathbf{s})$ extends to states $\mathbf{s} \neq \mathbf{s}_0$. Let us start with the state where $p(\mathbf{s}) > 0$ only for states \mathbf{s}_0 and $\mathbf{s}_1 = (1, 0, \dots, 0)$, which represents points with the first feature. Expanding around the state $w_{i,j} = 0$ for all i, j , we find (see Appendix)

$$\mathcal{L} = \sum_j [\bar{x}_j \log \bar{x}_j + (1 - \bar{x}_j) \log(1 - \bar{x}_j)] + \frac{1}{2} \sum_{j,j'} w_{1,j} D_{j,j'} w_{1,j'} + O(w^3) \quad (13)$$

with

$$D_{j,j'} = \mathbb{E}_{\mathbf{s}} [s_1] (1 - \mathbb{E}_{\mathbf{s}} [s_1]) \left[\overline{(x_j - \bar{x}_j)(x_{j'} - \bar{x}_{j'})} - \bar{x}_j(1 - \bar{x}_j) \delta_{j,j'} \right].$$

Inspection of the matrix \hat{D} reveals⁷ that the state $\hat{w} = 0$ is a saddle point. This means that second order statistics of the data does not provide information on which is the direction where the likelihood increases faster. This information is contained in $O(w^3)$ terms that depend on higher order moments (see Appendix). This is a further manifestation of the fact that relevant statistical information in structured data is carried by higher order moments (see e.g. [10]). The flat log-likelihood landscape is also responsible for the slow diffusive dynamics that characterises the initial stages during training.

Once the first feature is learned, the next features can be learned starting from the $\vec{w}_i = 0$ state, because the gradients of the log-likelihood are non-zero at this point. We refer to the Appendix for a detailed analysis. In brief, this depends on the fact that as soon as $\vec{w}_1 \neq 0$, the visible and the hidden variables are no longer independent and hence covariances between x_j and s_i are no longer zero.

2.3 The hierarchical features model

We recall that we interpret s_i as an indicator function of feature i , i.e. the distribution $p(\mathbf{x}|\mathbf{s})$ with $s_i = 1$ or 0 describes inputs \mathbf{x} with or without feature \vec{w}_i , respectively. The internal representation $p(\mathbf{s})$ encodes an *a-priori* organisation of the feature space which is consistent with the principles of maximal *a priori* ignorance and of maximal relevance:

⁶It is interesting to note that, by Jensen's inequality, $\mathcal{L} \geq \overline{\mathbb{E}_{\mathbf{s}} [\log p(\mathbf{x}|\mathbf{s})]}$. The lower bound $\overline{\mathbb{E}_{\mathbf{s}} [\log p(\mathbf{x}|\mathbf{s})]}$ only depends on the data through the first moment \bar{x}_j and it is maximal when a_j are given by Eq.(12) and $w_{i,j} = 0$ for all i, j .

⁷Notice that the diagonal elements of \hat{D} vanish, hence its trace also vanishes. This implies that there are positive and negative eigenvalues.

- 1) if \mathbf{x} has feature k then *i*) it may have any feature $i < k$ and *ii*) no information on whether feature $i < k$ is present or not is available, *a priori*.
- 2) $p(\mathbf{s})$ must be a distribution of maximal relevance.

The first principle can be stated as $P\{s_i = 1 | s_k = 1\} = \frac{1}{2}$ for all $i < k$. As a consequence, any configuration $\mathbf{s} = (s_1, \dots, s_{k-1}, 1, 0, \dots, 0)$ with $s_k = 1$ and $s_j = 0$ for all $j > k$ must have the same probability. This means that $p(\mathbf{s})$ must be a function of the largest index i for which $s_i = 1$, i.e. it must be a function of⁸

$$m_{\mathbf{s}} = \max\{i : s_i = 1\}. \quad (14)$$

The maximal relevance principle can be translated in the following distribution

$$p(\mathbf{s}) = \frac{1}{Z} e^{-g\mathcal{H}(\mathbf{s})}, \quad \mathcal{H}(\mathbf{s}) = \max\{m_{\mathbf{s}} - 1, 0\}, \quad (15)$$

where the partition function

$$Z = \sum_{\mathbf{s}} e^{-g\mathcal{H}(\mathbf{s})} = 1 + \frac{\xi^n - 1}{\xi - 1}, \quad \xi = 2e^{-g} \quad (16)$$

ensures normalisation. Indeed, Refs. [16, 4] show that, for a distribution of maximal relevance, the logarithm of the number of states with probability $p(\mathbf{s}) = e^{-E}$ should be a linear function of E . In our case, $p(\mathbf{s})$ depends on $m_{\mathbf{s}}$ and the number of states with $m_{\mathbf{s}} = k$ equals 2^{k-1} . This leads to Eq. (15).

Notice that, *a priori*, the points with just the first feature ($s_1 = 1$ and $s_i = 0$ for all $i > 1$) and the one without any feature ($s_i = 0$ for all i) are equiprobable. We call the distribution of Eq. (15) the *Hierarchical Feature Model* (HFM).

The expected value of the Hamiltonian \mathcal{H} is easily computed, as well as the entropy

$$\mathbb{E}_{\mathbf{s}}[\mathcal{H}] = \xi \left[\frac{n\xi^{n-1} - 1}{\xi^n + \xi - 2} - \frac{1}{\xi - 1} \right] \quad (17)$$

$$H[\mathbf{s}] = g\mathbb{E}_{\mathbf{s}}[\mathcal{H}] + \log \left(1 + \frac{\xi^n - 1}{\xi - 1} \right). \quad (18)$$

We take $\mathbb{E}_{\mathbf{s}}[\mathcal{H}]$ as an effective number of features used by the model.

In the limit $n \rightarrow \infty$, the model exhibits a phase transition at $g_c = \log 2$ (where $\xi = 1$). In the weak coupling phase ($g < g_c$) the model spans an extensive number of features and both the Hamiltonian and the entropy are extensive ($\mathcal{H}, H[\mathbf{s}] \sim n$). In the strong coupling phase ($g > g_c$) the typical number of features is finite and both \mathcal{H} and $H[\mathbf{s}]$ are of order one. Close to g_c we find

$$\mathbb{E}_{\mathbf{s}}[\mathcal{H}] \simeq \frac{n}{2} - 1 + \frac{1}{n+1} + O(n^2(g - g_c))$$

⁸The state $\mathbf{s}_0 = (0, \dots, 0)$ has $m_{\mathbf{s}} = 0$.

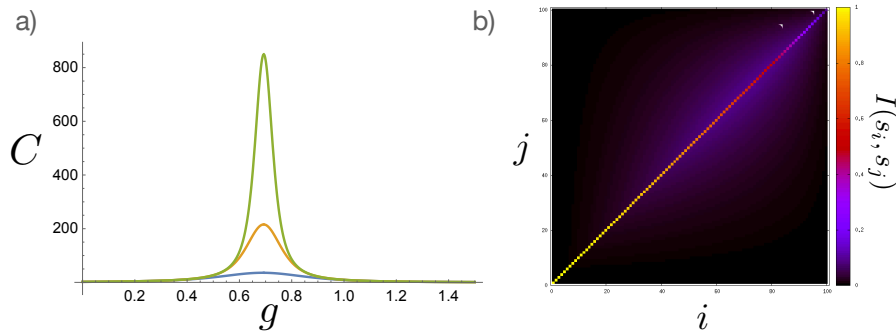


Figure 1: *a)* Specific heat of the HFM as a function of g for $n = 20$ (blue) 50 (orange) and 100 (green). *b)* Mutual information $I(s_i, s_j)$ (in bits) between different variables of the HFM, for $n = 100$ and $g = g_c$. The value on the diagonal is the entropy $H[s_i]$ of variable s_i .

which implies that for large n the crossover between the two regimes occurs in a region of size $|g - g_c| \sim 1/n$ around g_c . The phase transition is signalled by a divergence of the “specific heat” $C(g) = \mathbb{E}_{\mathbf{s}} \left[(\mathcal{H} - \mathbb{E}_{\mathbf{s}} [\mathcal{H}])^2 \right]$ at g_c , as shown in Fig. 1a). At g_c we find

$$C(g_c) = \frac{n(n-1)[n(n+5)-2]}{12(n+1)^2} \simeq \frac{n^2}{12} \quad (19)$$

when $n \rightarrow \infty$. This behaviour is consistent with the principle of maximal relevance [4] and with the one observed in neural tissues [17].

It is easy to compute moments of arbitrary order $\mathbb{E}_{\mathbf{s}} [s_i s_j \cdots s_\ell]$. Rather than showing uninformative formulas, we plot in Fig. 1b) the mutual information $I(s_i, s_j)$ between features i and j at the critical point. This shows that the presence of higher order features is not informative about the presence of lower order ones. Remarkably, this hold also at the critical point.

2.4 An expectation maximisation algorithm

In spite of the simplicity of the HFM, the calculation of the likelihood $\log p(\hat{\mathbf{x}}|\theta)$ or of its gradients is a complex task. It is in principle possible to devise Montecarlo Markov chain algorithms to sample the joint distribution $p(\mathbf{x}, \mathbf{s}|\theta)$ or the conditional one $p(\mathbf{s}|\mathbf{x}, \theta)$, in order to estimate the gradients. We explore, instead, deterministic algorithms that maximise the joint log-likelihood $\overline{\log p(\mathbf{x}, \mathbf{s}|\theta)}$, exploiting the fact that samples from $p(\mathbf{s})$ can be drawn independently of the data.

We resort to a classical variational argument which is at the basis of Expectation-

Maximisation (EM) algorithms [18]. Consider the maximisation of the free energy

$$F(Q, \theta) = \mathbb{E}_Q [\log p(\mathbf{x}, \mathbf{s}|\theta)] + H[Q] \quad (20)$$

$$= \log p(\mathbf{x}|\theta) - D_{KL}(Q||p(\mathbf{s}|\mathbf{x}, \theta)) \quad (21)$$

over the parameters θ and over the distribution $Q(\mathbf{s}|\mathbf{x})$. Here $\mathbb{E}_Q[\dots]$ stands for the expected value over the distribution Q . Inspection of the second line shows that the solution of this problem is equivalent to the maximisation of the likelihood over the parameters θ , because the optimum on Q is at $Q(\mathbf{s}|\mathbf{x}) = p(\mathbf{s}|\mathbf{x}, \theta)$.

If we expect that the solution $p(\mathbf{s}|\mathbf{x}, \theta)$ is sharply peaked around one value $\mathbf{s}(\mathbf{x})$, we can search for a maximum on the set of distributions

$$Q(\mathbf{s}|\mathbf{x}) = \delta_{\mathbf{s}, \mathbf{s}(\mathbf{x})}. \quad (22)$$

Within this class, the entropy of Q is zero ($H[Q] = 0$) and hence $F(Q, \theta)$ becomes the joint log-likelihood $\log p(\mathbf{x}, \mathbf{s}(\mathbf{x})|\theta)$. We shall then pursue the maximisation of the joint likelihood instead of the likelihood. This entails associating to each point $\mathbf{x}^{(a)}$ of the sample an internal state $\mathbf{s}^{(a)} = \mathbf{s}(\mathbf{x}^{(a)})$ in such a way as to maximise the joint log-likelihood

$$\frac{1}{N} \sum_{a=1}^N \log p(\mathbf{x}^{(a)}, \mathbf{s}^{(a)}|\theta) = \frac{1}{N} \sum_{a=1}^N \log p(\mathbf{x}^{(a)}|\mathbf{s}^{(a)}, \theta) + \frac{1}{N} \sum_{a=1}^N \log p(\mathbf{s}^{(a)}). \quad (23)$$

As in EM algorithms, the optimisation can be done in two steps: in the E-step one internal state $\mathbf{s}^{(a)}$ is associated to each data point $\mathbf{x}^{(a)}$. In the M-step the parameters θ are adjusted in order to maximise the joint log-likelihood Eq. (23) for fixed $\mathbf{s}^{(a)}$. The M-step only involves the conditional distribution $p(\mathbf{x}|\mathbf{s}, \theta)$. Indeed the second term in the r.h.s. of Eq. (23) is independent of θ and it can be written as

$$\frac{1}{N} \sum_{a=1}^N \log p(\mathbf{s}^{(a)}) = -H[q] - D_{KL}(q(\mathbf{s})||p(\mathbf{s})) \quad (24)$$

where $H[q]$ is the entropy of the *clamped state distribution*

$$q(\mathbf{s}) = \frac{1}{N} \sum_{a=1}^N \delta_{\mathbf{s}, \mathbf{s}^{(a)}} \quad (25)$$

i.e. the distribution which is induced by the data in the internal layer. The assignment of internal states $\mathbf{s}^{(a)}$ in the the E-step then strikes a balance between describing optimally the data (first term in Eq. 23) and driving the clamped state distribution as close as possible to $p(\mathbf{s})$ (second term in Eq. 23). From a thermodynamic perspective, the E-step involves a relaxation process where the occupation of energy levels changes. This is associated to heat exchange processes⁹.

⁹Whereas the M-step corresponds to a processes where work is done.

The distribution of clamped states provides an estimate of the distribution $p_\infty(\mathbf{s}) \approx q(\mathbf{s})$ of internal states after training, which are initially distributed according to $p_0(\mathbf{s}) = p(\mathbf{s})$ (see Eq. 8). From a thermodynamic perspective, the data drives the state of the hidden layer out of equilibrium and the second term in Eq. (24) measures the minimal thermodynamic cost involved.

3 Numerical experiments

We run extensive training experiments on different datasets. These include:

- the MNIST, EMNIST and FASHION datasets are collections of grayscale images of 28×28 pixels ($m = 784$). We normalize each pixel into the range of 0 to 1. The MNIST dataset contains $N = 6 \cdot 10^4$ handwritten digital images of the digits from 0 to 9 [19]. We consider the ByClass version of EMNIST¹⁰, which is a collection of $N = 814255$ handwritten character images, containing [0-9] digits, [A-Z] uppercase character and [a-z] lowercase characters. The FASHION dataset¹¹ consists of Zalando’s article images [20] ($N = 6 \cdot 10^4$).
- Big Five Personality Test (Big5)¹² is a questionnaire with $m = 50$ questions that are believed [21] to characterise the personality of individuals along five traits: extraversion, agreeableness, openness, conscientiousness, and neuroticism. Respondents give a score from 1 to 5 to each question, which we rescale to the interval $[0, 1]$. The dataset is composed of $N = 1015342$ compiled questionnaires.
- the Amazon Jewelry Reviews¹³ is a text database. We choose the reviews whose length is larger than or equal to 200 words and select the top $m = 5000$ words to generate the corresponding feature vector for each review by using the tf-idf method [22]. We utilize these features as our data.

We shall first address the issue of the dependence of the internal representation on the data in the next Section, and then discuss an approach based on learning features incrementally.

3.1 Independence of the internal representation on the data

We explored different algorithms. All the result of this Section are derived from datasets of $N = 6 \cdot 10^4$ data points, so as to make comparison across datasets more transparent. As discussed above, these are based on an expectation-maximisation strategy. In Algorithm

¹⁰ Available at <https://www.nist.gov/itl/products-and-services/emnist-dataset>.

¹¹ Available at <https://github.com/zaladoresearch/fashion-mnist>.

¹² Available at <https://www.kaggle.com/datasets/tunguz/big-five-personality-test>.

¹³ Downloaded from https://s3.amazonaws.com/amazon-reviews-pds/tsv/amazon_reviews_us_Jewelry_v1.00.tsv.gz.

As we exploit the fact that $p(\mathbf{s})$ is fixed, in order to draw a sample $\hat{\mathbf{s}} = (\mathbf{s}^{(1)}, \dots, \mathbf{s}^{(N)})$ of N internal states at the outset. Then we alternate M-steps based on the usual gradient ascent with E-steps in which internal states $\mathbf{s}^{(i)}$ are assigned to data-points $\mathbf{x}^{(j)}$ in order to maximise the joint log-likelihood. In practice, an assignment coincides with a permutation $j = \pi_i$ of the integers $(1, \dots, N)$. In Algorithm B the initial configuration of $\hat{\mathbf{s}}$ evolves in the E-step by single “spin flips” where one of the hidden variables $s_i^{(\ell)} \rightarrow 1 - s_i^{(\ell)}$ is changed in order to increase the (joint) likelihood. Further details on the algorithms is given in the Appendix.

We consider different hidden state distributions $p(\mathbf{s})$. The simplest is the uniform distribution, which assigns the same probability $p(\mathbf{s}) = 2^{-n}$ to each internal state. We also consider the HFM at criticality (ie. with $g = \log 2$). Finally, we derive $p(\mathbf{s})$ by training a RBM on each dataset and marginalising over \mathbf{x} . The models $p(\mathbf{s})$ obtained in this way from one dataset will be used as internal representations in the training of other data sets.

The results are summarised in Table 3.1 and Fig. 2 for representative cases. We find that in all architectures where $p(\mathbf{s})$ is fixed the reconstruction error is small, although it is not as small as that of RBMs. The running time is of the same order of that of RBMs.

The results confirm that a $p(\mathbf{s})$ with a broad distribution of $\log p(\mathbf{s})$ performs better than one with a narrow distribution. Indeed the reconstruction error when $p(\mathbf{s})$ is the HFM or is obtained from RBMs trained on different datasets is smaller than the one found for $p(\mathbf{s}) = 2^{-n}$ (Random). Visual inspection of the digits recalled (Fig. 2 d) or generated (Fig. 2 e) from the random model corroborates this conclusion (compare c to d, and e to f in Fig. 2).

Still the performance of the Random model is surprisingly good, as this is expected to combine features randomly. Closer inspection in $p(\mathbf{x}|\mathbf{s})$ reveals that this behaviour is likely related to the fact that only few features \vec{w}_i have relatively large values whereas most of the features have small values of $|w_{i,j}|$. Hence whether one of such “weak” feature is present ($s_i = 1$) or not ($s_i = 0$) does not affect much the distribution of \mathbf{x} .

A further interesting observation is that images generated from the HFM exhibit combination of patterns which are not present in the training datasets, such as pants with sleeves (3rd image in the 2nd row of Fig. 2 f). We could not observe such combination of patterns in images generated from the RBM.

$p(\mathbf{s})$	Data	Algorithm	Error	Time
RBM	REVIEWS	CD1	$1.91 \cdot 10^{-4}$	28.2
	MNIST	CD1	0.0098	14.4
	EMNIST	CD1	0.0133	14.4
	FASHION	CD1	0.0144	15.7
Random	REVIEWS	A	$2.00 \cdot 10^{-4}$	30.5
	MNIST	A	0.0471	24.9
	EMNIST	A	0.0570	25.6
	FASHION	A	0.0405*	50
Random	REVIEWS	B	$1.78 \cdot 10^{-4}$	20.4
	MNIST	B	0.0313	9.3
	EMNIST	B	0.0384	9.3
	FASHION	B	0.0278	9.5
HFM	REVIEWS	A	$1.87 \cdot 10^{-4}$	35.3
	MNIST	A	0.0448	18.5
	EMNIST	A	0.0556	18.4
	FASHION	A	0.0339	23.2
Big5	REVIEWS	A	$1.88 \cdot 10^{-4}$	40
	MNIST	A	0.0479	22.4
	EMNIST	A	0.0617	22.9
	FASHION	A	0.0409	24
MNIST	REVIEWS	A	$1.85 \cdot 10^{-4}$	35.8
	EMNIST	A	0.0543	31
	FASHION	A	0.0324*	63.6
EMNIST	REVIEWS	A	$1.86 \cdot 10^{-4}$	35
	MNIST	A	0.0434	33.3
	FASHION	A	0.0333	61.2
FASHION	REVIEWS	A	$1.85 \cdot 10^{-4}$	42.9
	MNIST	A	0.0401	37.7
	EMNIST	A	0.0515	32.5

Table 1: Reconstruction error and running time (minutes) of different algorithms with fixed hidden probability models and different datasets. Each algorithm is run for 100 epochs. Random corresponds to a uniform $p(\mathbf{s}) = 2^{-n}$ whereas HFM is the Hierarchical Feature model discussed in Section 2.3. Big5, MNIST, EMNIST and FASHION in the first column refer to the case where $p(\mathbf{s})$ is obtained from an RBM trained on the respective dataset. The number of hidden units is $n = 100$ for all models except Big5 for which $n = 20$.

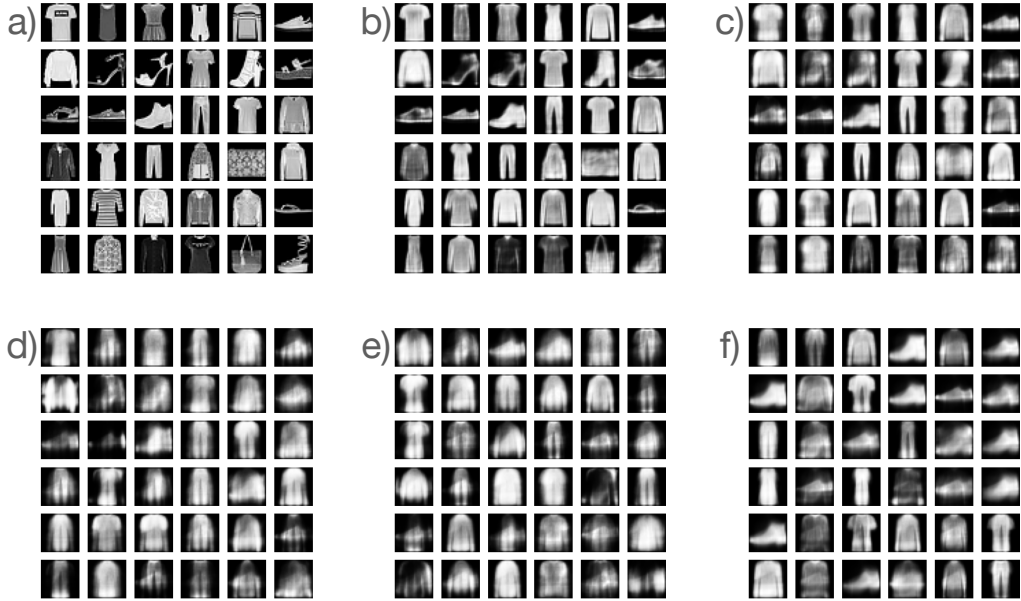


Figure 2: Comparison of original sample picture of the FASHION dataset (a) with those obtained from different trained model. Panels b), c) and d) refers to recall, i.e. when a picture is generated from an internal state \mathbf{s} which is sampled from $p(\mathbf{s}|\mathbf{x})$, where \mathbf{x} is one of the original pictures. Pictures e) and f) correspond to figures generated from states \mathbf{s} drawn at random from $p(\mathbf{s})$. b) correspond to recall from a trained RBM on FASHION dataset, c) to recall when $p(\mathbf{s})$ is the distribution of hidden states of an RBM trained on MNIST and d) to recall when $p(\mathbf{s}) = 2^{-n}$ is uniform. In e) figures are generated from an hidden state randomly drawn from $p(\mathbf{s}) = 2^{-n}$ while in f) the hidden state is sampled from the HFM. In all cases $n = 100$.

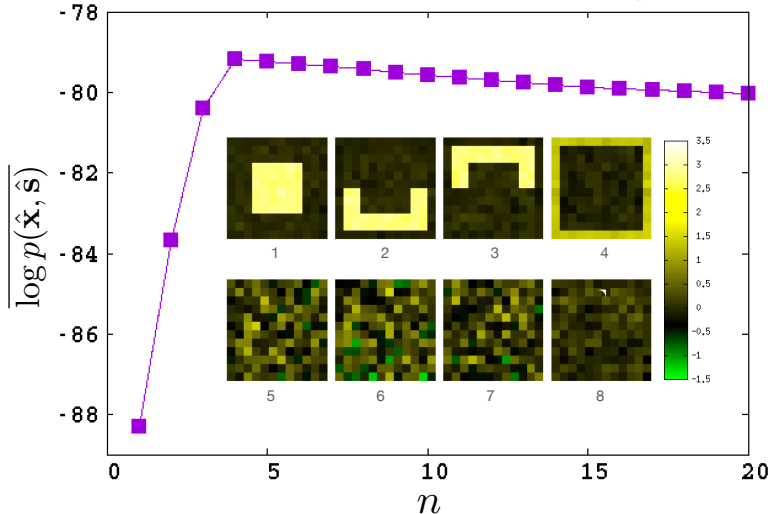


Figure 3: Recovery of the structure of a HFM from a dataset of $N = 6000$ points. The HFM used to generate the data contains four features, for each of these $w_{i,j}$ in $p(\mathbf{x}|\mathbf{s})$ takes values $\log 4 \simeq 1.39$ on a subset of the pixels and $w_{i,j} = 0$ otherwise ($a_j = 0$ for all j). This subset is the central square of 6×6 pixels for the first feature, the lower (upper) half of the pixels at a distance 2 or 3 from the border for the second (third) feature, and the pixels on the outer perimeter for the fourth. The main plot shows that in-sample likelihood as a function of the number n of features, for $g = 0.70 \simeq g_c$. The inset shows the features recovered for $n = 8$.

3.2 Learning one feature at a time

In this Section we discuss the results of an algorithm that learns one feature at a time, based on the HFM. Given the trained model with $n - 1$ features, we add the n^{th} feature and train the model with n features. The algorithm is similar to algorithm B in the previous section, where, in the E-step, the internal state is adjusted to $\mathbf{s}^{(i)} = \arg \max_{\mathbf{s}} \log p(\mathbf{x}^{(i)}, \mathbf{s}|\theta)$, for each data point $\mathbf{x}^{(i)}$. At odd with algorithms in the previous section, here we do not rely on mini-batches. Hence the resulting algorithm is fully deterministic. More details on the algorithm are given in the Appendix.

3.2.1 A synthetic dataset

We start by testing the ability of the algorithm to recover a structure of hierarchical features from a dataset generated by the HFM model itself. The data consists of $N = 6000$ images of 12×12 black or white pixels ($x_j = 0$ or 1) formed combining the four features shown in Fig. 3. As shown, the joint likelihood sharply increases with n when there are less than four features, but it decreases when $n > 4$. The first four recovered features coincide with

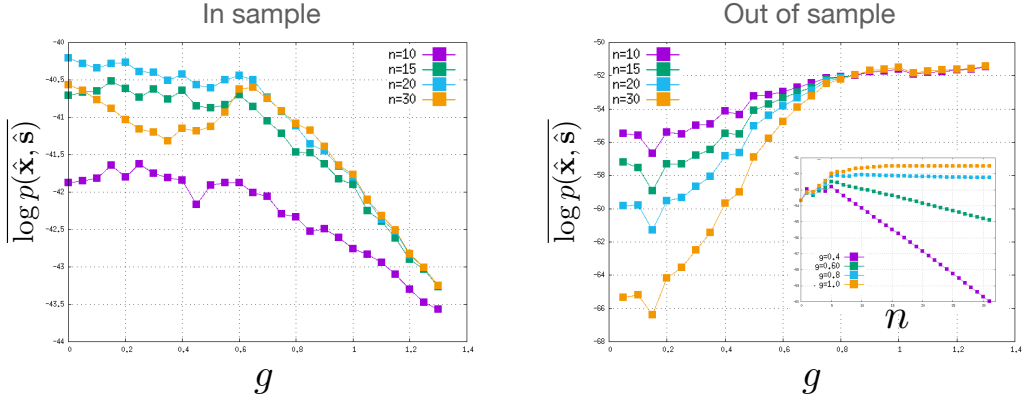


Figure 4: Joint log-likelihood in-sample (left) and out-of-sample (right) for the rMNIST dataset, for networks with different numbers (n) of hidden nodes, as a function of the parameter g . The inset in the left panel shows the out-of-sample joint log-likelihood as a function of n , for different values of g .

those used in the model. The features of order $i > 4$ appear to be noisy and they become weaker moving down the hierarchy.

3.2.2 MNIST

We trained the HFM on the MNIST dataset of hand written digits. An extensive analysis has been carried out for a reduced version of this dataset, that we call the rMNIST, which was also used in a previous publication [4].

Fig. 4 shows the in-sample and out-of-sample likelihood as a function of g for different values of n . These have opposite behaviours: while the in-sample likelihood generally decreases with g , the out-of-sample likelihood increases. In both cases, the behaviour changes qualitatively when $g \approx g_c \simeq 0.7$. For $g > g_c$, the out-of-sample likelihood levels off to a nearly constant value, for all n . In the same region, the in-sample likelihood decreases sharply with g , whereas it hovers around a constant value for $g < g_c$.

The inset shows that for $g < g_c$ the statistical accuracy degrades upon adding more features, suggesting that the model is overfitting the data. For $g > g_c$ instead the out-of-sample log-likelihood levels off to a constant value as n increases. This is related to the fact that the effective number of features \mathcal{H} is finite for $g > g_c$ and it diverges for $g \leq g_c$.

Fig. 5 provides a complementary perspective on the trained HFM. First (left panel of Fig. 5) it shows that the occupation of internal states \mathbf{s} is very far from the equilibrium distribution $p(\mathbf{s})$ for $g < g_c$ whereas $q(\mathbf{s})$ stays close to $p(\mathbf{s})$ for $g > g_c$. This implies that the generative performance of the model is expected to be poor when $g < g_c$, because the distribution $q(\mathbf{s})$ induced by the data is far from $p(\mathbf{s})$, and it is expected to improve for $g > g_c$. Second it shows that the occupation of internal states changes smoothly for $g > g_c$

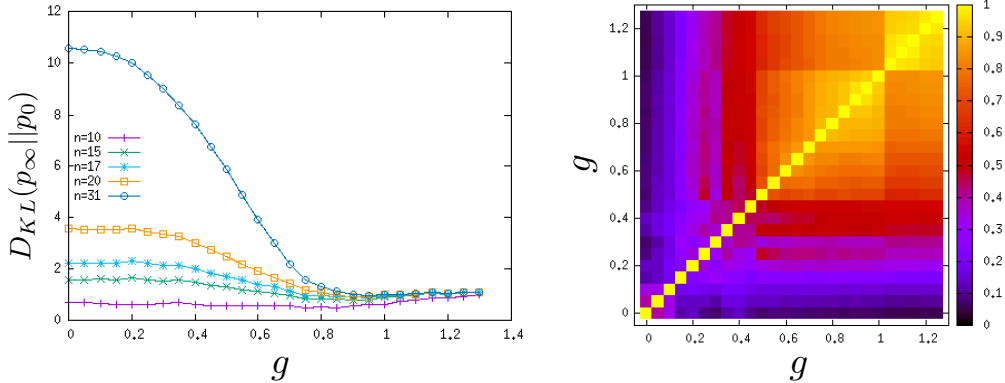


Figure 5: Left: Kullback-Leibler divergence between the final distribution $p_\infty(\mathbf{s}) \approx q(\mathbf{s})$ after training, and the initial one $p_0(\mathbf{s}) = p(\mathbf{s})$. Right: overlap between the internal representations of the rMNIST dataset for different values of g . The overlap between two configurations $\mathbf{s}_\alpha^{(a)}$ and $\mathbf{s}_\beta^{(a)}$ is computed as $q_{\alpha,\beta} = \frac{1}{nN} \sum_{i,a} s_{i,\alpha}^{(a)} s_{i,\beta}^{(a)}$, where $s_{i,\alpha}^{(a)}$ is the value of the i^{th} spin of the internal representation of the a^{th} data point $\mathbf{s}_\alpha^{(a)}$.

but it changes abruptly for $g < g_c$ (right panel of Fig. 5).

The features learned in the HFM converge quickly to an asymptotic value when more features or more data-points are added. Fig. 6 (left) plots the distance

$$d(\vec{w}_i, \vec{w}'_i) = 1 - \frac{\vec{w}_i \cdot \vec{w}'_i}{|\vec{w}_i| |\vec{w}'_i|} \quad (26)$$

between the i^{th} feature learned with N' data-points and the same feature learned with the whole dataset ($N = 60000$). This suggests that low order features are learned first (i.e. with few data points) whereas higher order ones need more data to converge.

A similar analysis is reported in the right panel of Fig. 6, when N is fixed but the number n of features changes. For the HFM the distance of \vec{w}_i when n features are learned to its value when the final number of features are learned is shown in the part below the diagonal of the plot in the right panel of Fig. 6. For comparison we show the same plot for a RBM in the upper diagonal part (with axes inverted). While for the latter the introduction of a new feature perturbs the already learned ones, for the HFM low order features remain stable even when further high order features are learned.

The robustness of the internal representation also manifests in the fact that features change very little as the parameter g varies. This is shown in Fig. 7. The hierarchical organisation of features is also evident in the fact that features become weaker and weaker as their order increases. A further evidence of this, is that relevant information on the data, such as the value of the digits in the MNIST case, is mostly contained in low order features, as shown in Fig. 7 (right).

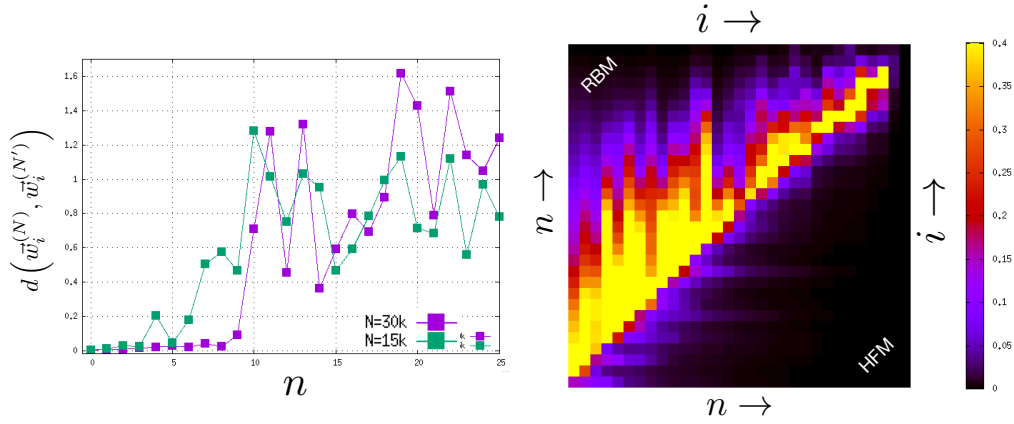


Figure 6: Left: distance $d(\vec{w}_i, \vec{w}_i')$ between the i^{th} feature \vec{w}_i learned with N data points and the one (\vec{w}_i') learned with the whole rMNIST dataset ($6 \cdot 10^4$ data points). The green points correspond to $N = 1.5 \cdot 10^4$, the violet ones to $N = 3 \cdot 10^4$. Right: Distance $d(\vec{w}_i^{(n)}, \vec{w}_i)$ between the i^{th} feature $\vec{w}_i^{(n)}$ in a machine with n features and the i^{th} feature \vec{w}_i in a machine with 31 features. The lower triangular data refer to the HFM (i increases from bottom to top and n from left to right). The upper triangular data refer to a RBM (i increases from left to right and n from bottom to top).

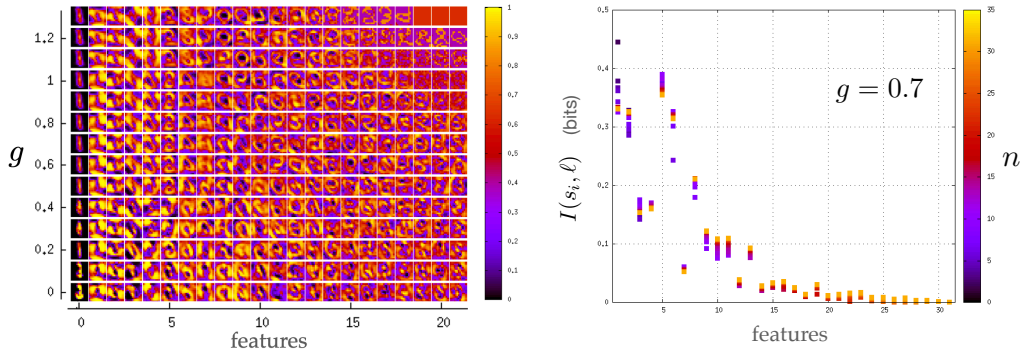


Figure 7: Left: the first 21 features of a HFM with $n = 31$ features, for different values of g . Each pixel reports the value of $(1 + e^{-w_{i,j}})^{-1}$ so that its value is in $[0, 1]$. The 0^{th} feature corresponds to a_j . Right: Mutual information between labels ℓ and the i^{th} feature s_i , for $g = 0.7$. Different values of n correspond to different colours (see scale on the right).

3.2.3 The Big Five personality test

We run our algorithm on the Big Five dataset separately for respondents of different countries. In all cases we find that the log-likelihood reaches a maximum at six or seven features and then it decreases if more features are added (see Fig. 8 right). This suggests that the optimal number of features is close to five. Closer inspection of the features shows that, for all countries except two (India and Mexico), each of the first five features significantly concentrates on the sets of ten questions that correspond to one of the five traits. The two countries where the correspondence between features and traits is not sharp (India and Mexico) also exhibit lower values of the log-likelihood. The ranking of the traits agrees across some countries and it differs in others. Whether or not these results unveil cultural differences across countries is an issue that goes beyond the scope of this paper. The main purpose of this exercise is to show that the HFM uncovers a clear structure of features that in most of the cases coincides with the one expected, where the five traits emerge.

4 Discussion

This paper proposes a principled approach to machine learning for probabilistic single layer networks which conforms to Occam razor. We restrict attention to binary data but the extension to continuous variables \mathbf{x} is straightforward¹⁴. In the models we study, we take the internal representation fixed and learn only the way in which this projects to the data. Approaches where the interactions between the internal variables are not learned, such as those reviewed in Ref. [8], have been studied mostly in supervised learning. Here instead we address unsupervised learning tasks. In addition, we draw on recent results that suggest that optimal internal representations satisfy a principle of maximal relevance [3]. This implies that optimal performance is achieved when the internal representation is close to a critical state, as observed in both artificial (see e.g. [23, 24, 25]) as well as in biological learning [26, 27].

The approach proposed in this paper is similar in spirit to sparse dictionary learning [28, 29], which aims at describing different data points in the dataset as different combinations of the same set (the dictionary) of features. In our case, the dictionary coincides with the set of features $\mathcal{D} = \{\vec{w}_i\}_{i=1}^n$ whereas \mathbf{s} specifies how features are combined. In our case, features do not have to satisfy any *a priori* property (e.g. orthogonality), but they inherit the organisation imposed by $p(\mathbf{s})$.

It's important to remark that we were not able to exhibit algorithms with a computational performance superior to that of state-of-the-art algorithms such as RBMs. This was not our aim to start with. Yet this is a clear shortcoming of the results presented in this paper that we hope can be overcome in future research.

¹⁴It can for example be achieved by taking $p(\mathbf{x}|\mathbf{s})$ as a Gaussian distribution with a mean $\mathbb{E}[x_j] = a_j + \sum_i s_i w_{i,j}$ that depends on the features.

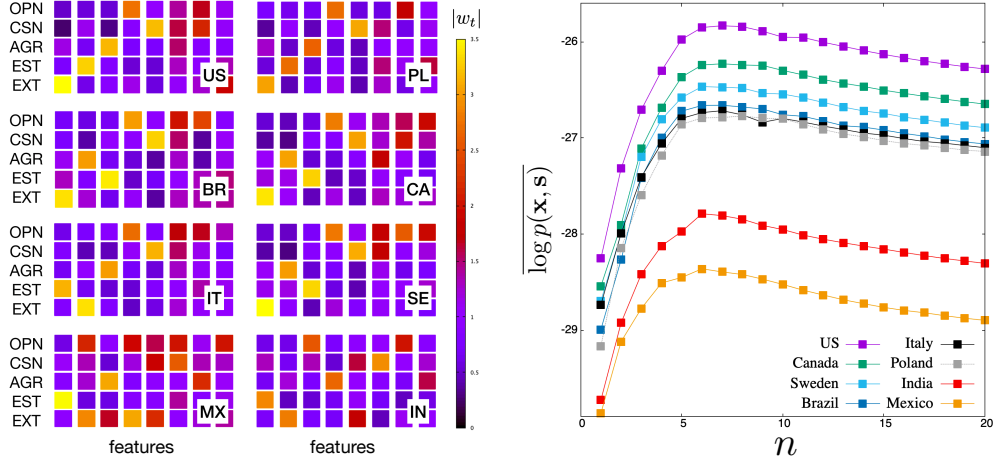


Figure 8: Left: Average size of the weights $w_{i,j}$ corresponding to the five blocks of ten questions relative to the five traits: openness (OPN), conscientiousness (CSN), agreeableness (AGR), neuroticism (EST) and extraversion (EXT). The 8 panels shows that the top five features coincide with the first five traits for all countries except India (IN) and Mexico (MX). The figure displays on a colour scale the value the average weight strength $|w_{i,t}| = \sqrt{\frac{1}{10} \sum_{j \in t} w_{i,j}^2}$ that feature i attributes to questions related to one of the traits t . The number of data points for the different countries is $N = 472320, 5481, 4570, 9389, 4008, 53663, 9122$ and 13899 for United States (US), Brazil (BR), Italy (IT), Mexico (MX), Poland (PL), Canada (CA), Sweden (SW) and India (IN). Right: In-sample joint log-likelihood for the same datasets as a function of the number n of features, for $g = g_c$.

It is interesting to contrast architectures where the internal representation $p(\mathbf{s})$ is fixed, such as those studied here, to those where it is learned, as in RBMs. The weights of RBMs correspond to generic features, such as localised filters. Indeed, the weights learned from one dataset can reasonably well represent a different dataset, as shown in Fig. 9 (see caption). This suggests that the weights \vec{u}_i do not carry information on the data, which is stored in the way the weights are combined to produce the output, i.e. in $p(\mathbf{s})$. The same trained RBM can describe both the data with which it has been trained as well as other data. When it comes to its generative performance, the RBM produces outputs which are similar to the data it has been trained only. These indeed are the outputs that correspond to typical internal states \mathbf{s} . Outputs such as those of Fig. 9 b), correspond to (EMNIST clamped) states \mathbf{s}_E which are very atypical. Indeed, we found that the probability $p(\mathbf{s}_E)$ of EMNIST clamped states \mathbf{s}_E is typically a factor $\sim 10^{-52}$ smaller than that of the clamped hidden states corresponding to the MNIST dataset with which the RBM was trained. This property is important for applications of transfer learning because it suggests that, in supervised learning, biasing the internal layer by training only the output layer may be enough to achieve a reasonably good classifier. It also suggests low degrees of plasticity, i.e. that weights should change by a small amount when the RBM is further trained on a different dataset. This is reminiscent of suppressed levels of experience dependent plasticity after development in sensory brain areas [30], such as the primary visual cortex, which also encode representations in terms of generic features.

The fact that weights encode generic features in RBMs is consistent with the non-uniqueness of the learned representation $p(\mathbf{s})$. A RBM generates one out of a manifold of possible models that accurately describe a dataset. Which one the training process selects depends on the random initial conditions and on the details of the training process.

By contrast, when the internal representation $p(\mathbf{s})$ is fixed at the outset, the trained weights necessarily encode very specific features of the dataset. In addition, this reduces considerably the space of probability distributions that training algorithms have to explore, thereby reducing the degeneracy of solutions also. For these architectures, we found that deterministic gradient based algorithms can be used to learn the parameters. At the same time, we argued that architectures where the internal representation is fixed enable functions that go beyond the mere generalisation, which are similar to higher cognitive functions such as generating objects which have never been seen (as in imagination or dreaming) or drawing analogies between data learned in different domains.

Architectures where the internal representation $p(\mathbf{s})$ is shaped during training, such as RBMs, are consistent with an empiricist approach to learning, that starts from a blank slate initial state and all knowledge comes from experience. By contrast, architectures with a fixed internal representation are reminiscent of nativism approaches, which assume an innate “universal structure”, such as the one hypothesised by Chomsky for language [31]. It is tempting to conclude that both architectures are used in more complex learning machines such as the brain, where brain regions responsible for the encoding of stimuli (e.g. the primary visual cortex) have RBM type architectures, whereas deeper cortical regions

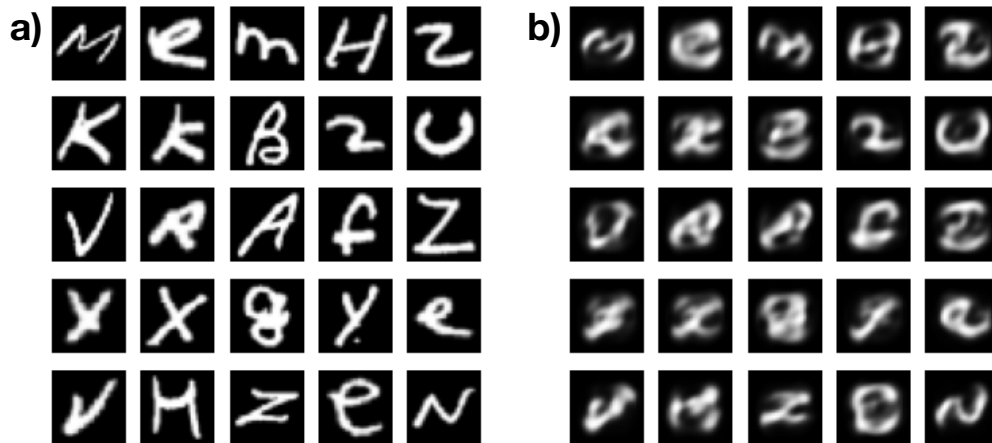


Figure 9: a) A sample of characters from the EMNIST dataset. b) output of a RBM trained on the MNIST dataset when clamped on the EMNIST characters in a). These are obtained finding the most likely internal state $\mathbf{s}_E = \arg \max_{\mathbf{s}} p(\mathbf{x}_E, \mathbf{s})$ of an RBM where the visible layer is fixed to an EMNIST character \mathbf{x}_E . In b) we show the plot of $\mathbb{E}[\mathbf{x}|\mathbf{s}_E]$ generated by the RBM. The RBM has $n = 100$ hidden variables and is trained on MNIST for 100 epochs with mini-batches of 50 data points and contrastive divergence with $k = 100$.

responsible for higher cognitive functions are endowed by a fixed internal representation. Indeed, mapping data onto an existing structure is a type of learning which resembles what we commonly call “understanding” [32]. This points to the intriguing hypothesis that “universal” (data-independent) internal representations may emerge spontaneously in deep layers of learning architectures, which will be the subject of future research.

References

- [1] Chiyuan Zhang, Samy Bengio, Moritz Hardt, Benjamin Recht, and Oriol Vinyals. Understanding deep learning (still) requires rethinking generalization. *Communications of the ACM*, 64(3):107–115, 2021.
- [2] Song Mei and Andrea Montanari. The generalization error of random features regression: Precise asymptotics and the double descent curve. *Communications on Pure and Applied Mathematics*, 2019.
- [3] Matteo Marsili and Yasser Roudi. Quantifying relevance in learning and inference. *Physics Reports*, 963:1–43, 2022.

- [4] O Duranthon, M Marsili, and R Xie. Maximal relevance and optimal learning machines. *Journal of Statistical Mechanics: Theory and Experiment*, 2021(3):033409, 2021.
- [5] J Song, M Marsili, and J Jo. Resolution and relevance trade-offs in deep learning. *Journal of Statistical Mechanics: Theory and Experiment*, 2018(12):123406, dec 2018.
- [6] Ali Rahimi and Benjamin Recht. Random features for large-scale kernel machines. *Advances in neural information processing systems*, 20, 2007.
- [7] Liyanaarachchi Lekamalage Chamara Kasun, Hongming Zhou, G-B Huang, and Chi Man Vong. Representational learning with elms for big data. *IEEE intelligent systems*, 28(6):31–34, 2013.
- [8] Jose C Principe and Badong Chen. Universal approximation with convex optimization: Gimmick or reality? 10(2):68–77, 2015.
- [9] Geoffrey E Hinton. A practical guide to training restricted boltzmann machines. In *Neural networks: Tricks of the trade*, pages 599–619. Springer, 2012.
- [10] Alessandro Ingrosso and Sebastian Goldt. Data-driven emergence of convolutional structure in neural networks. *arXiv preprint arXiv:2202.00565*, 2022.
- [11] Jorge Fernandez-de Cossio-Diaz, Simona Cocco, and Remi Monasson. Disentangling representations in restricted boltzmann machines without adversaries. *arXiv preprint arXiv:2206.11600*, 2022.
- [12] R Shwartz-Ziv and N Tishby. Opening the black box of deep neural networks via information. *arXiv preprint arXiv:1703.00810*, 2017.
- [13] Aurélien Decelle, Cyril Furtlehner, and Beatriz Seoane. Equilibrium and non-equilibrium regimes in the learning of restricted boltzmann machines. *Advances in Neural Information Processing Systems*, 34:5345–5359, 2021.
- [14] Massimiliano Esposito and Christian Van den Broeck. Second law and landauer principle far from equilibrium. *EPL (Europhysics Letters)*, 95(4):40004, 2011.
- [15] Sridhar Mahadevan. Imagination machines: A new challenge for artificial intelligence. In *Proceedings of the AAAI Conference on Artificial Intelligence*, volume 32, 2018.
- [16] Ryan John Cubero, Junghyo Jo, Matteo Marsili, Yasser Roudi, and Juyong Song. Statistical criticality arises in most informative representations. *Journal of Statistical Mechanics: Theory and Experiment*, 2019(6):063402, jun 2019.

- [17] G Tkačik, T Mora, O Marre, D Amodei, S E Palmer, M J Berry, and W Bialek. Thermodynamics and signatures of criticality in a network of neurons. *Proceedings of the National Academy of Sciences*, 112(37):11508–11513, 2015.
- [18] Radford M Neal and Geoffrey E Hinton. A view of the em algorithm that justifies incremental, sparse, and other variants. In *Learning in graphical models*, pages 355–368. Springer, 1998.
- [19] Yann LeCun. The mnist database of handwritten digits. <http://yann.lecun.com/exdb/mnist/>, 1998.
- [20] Han Xiao, Kashif Rasul, and Roland Vollgraf. Fashion-mnist: a novel image dataset for benchmarking machine learning algorithms. *arXiv preprint arXiv:1708.07747*, 2017.
- [21] Lewis R Goldberg. The structure of phenotypic personality traits. *American psychologist*, 48(1):26, 1993.
- [22] Ricardo Baeza-Yates, Berthier Ribeiro-Neto, et al. *Modern information retrieval*, volume 463. ACM press New York, 1999.
- [23] Chris G Langton. Computation at the edge of chaos: Phase transitions and emergent computation. *Physica D: Nonlinear Phenomena*, 42(1-3):12–37, 1990.
- [24] Nils Bertschinger and Thomas Natschläger. Real-time computation at the edge of chaos in recurrent neural networks. *Neural computation*, 16(7):1413–1436, 2004.
- [25] Andrea Roli, Marco Villani, Alessandro Filisetti, and Roberto Serra. Dynamical criticality: overview and open questions. *Journal of Systems Science and Complexity*, 31(3):647–663, 2018.
- [26] John M Beggs. The criticality hypothesis: how local cortical networks might optimize information processing. *Philosophical Transactions of the Royal Society A: Mathematical, Physical and Engineering Sciences*, 366(1864):329–343, 2008.
- [27] Woodrow L Shew and Dietmar Plenz. The functional benefits of criticality in the cortex. *The neuroscientist*, 19(1):88–100, 2013.
- [28] Kenneth Kreutz-Delgado, Joseph F Murray, Bhaskar D Rao, Kjersti Engan, Te-Won Lee, and Terrence J Sejnowski. Dictionary learning algorithms for sparse representation. *Neural computation*, 15(2):349–396, 2003.
- [29] John Wright, Yi Ma, Julien Mairal, Guillermo Sapiro, Thomas S Huang, and Shuicheng Yan. Sparse representation for computer vision and pattern recognition. *Proceedings of the IEEE*, 98(6):1031–1044, 2010.

- [30] Nicoletta Berardi, Tommaso Pizzorusso, and Lamberto Maffei. Critical periods during sensory development. *Current opinion in neurobiology*, 10(1):138–145, 2000.
- [31] Noam Chomsky et al. *Reflections on language*. Temple Smith London, 1976.
- [32] A. Ingrosso. Private Communication, 2023.
- [33] Juan M R Parrondo, Jordan M Horowitz, and Takahiro Sagawa. Thermodynamics of information. *Nature physics*, 11(2):131, 2015.
- [34] Domingos SP Salazar. Nonequilibrium thermodynamics of restricted boltzmann machines. *Physical Review E*, 96(2):022131, 2017.
- [35] Roy Jonker and Anton Volgenant. A shortest augmenting path algorithm for dense and sparse linear assignment problems. *Computing*, 38(4):325–340, 1987.

5 Acknowledgments

MM thanks Iacopo Mastromatteo who brought to his attention the HFM as a model of maximal relevance. We thank Roberto Mulet for interesting discussions in the initial stages of this work, Alessandro Ingrosso and Davide Zoccolan for insightful comments. Rongrong Xie acknowledges a fellowship from the China Scholarship Council (CSC) under Grant CSC No. 202006770018.

A Thermodynamic efficiency of learning

Recent results on the thermodynamics of information processing systems [33] set precise thermodynamic limits to exchanges of information, heat and work. This opens the possibility to quantify the costs of learning, a program that has been carried out so far only for specific systems (see e.g. [34]).

Here we present a general argument suggesting that a design of learning machines where the internal representation $p(\mathbf{s})$ does not need to be learnt implies considerable savings on the thermodynamic costs of learning. My objective is to put this conjecture on firmer ground. Consider a generic training process. In the initial state, the data \mathbf{x} and the internal representation \mathbf{s} are independent random variables, i.e. the initial distribution is given by $p_0(\mathbf{x}, \mathbf{s}) = p_0(\mathbf{x})p_0(\mathbf{s})$ where $p_0(\mathbf{x})$ is the (unknown) data distribution and $p_0(\mathbf{s})$ is the marginal distribution of the internal state of the machine. From a thermodynamic perspective, training involves putting the two systems (the data and the machine) into contact, at a fixed temperature, and adjusting the weights of the machine until the data and the machine converge to a state $p_\infty(\mathbf{x}, \mathbf{s}) = p_\infty(\mathbf{x}|\mathbf{s})p_\infty(\mathbf{s})$, which is such that the final marginal distribution of \mathbf{x} well approximates the data distribution, i.e. $p_\infty(\mathbf{x}) \approx p_0(\mathbf{x})$. It seems reasonable to assume that the further apart the initial state is from the final state,

the higher the thermodynamic costs (i.e. the entropy production). Esposito and Van den Broeck [14] suggest that the minimal work (in units of $k_B T$) needed to drive the system from the initial equilibrium state to the final state is given by the non-equilibrium free-energy difference, which in turn is given by the Kullback-Leibler divergence between the final and the initial state

$$D_{KL}(p_\infty(\mathbf{x}, \mathbf{s}) || p_0(\mathbf{x})p_0(\mathbf{s})) = \sum_{\mathbf{x}, \mathbf{s}} p_\infty(\mathbf{x}, \mathbf{s}) \log \frac{p_\infty(\mathbf{x}, \mathbf{s})}{p_0(\mathbf{x})p_0(\mathbf{s})} \quad (27)$$

$$= \sum_{\mathbf{x}, \mathbf{s}} p_\infty(\mathbf{x}, \mathbf{s}) \log \frac{p_\infty(\mathbf{x}|\mathbf{s})}{p_0(\mathbf{x})} + D_{KL}(p_\infty(\mathbf{s}) || p_0(\mathbf{s})) \quad (28)$$

Under the assumption that the final marginal distribution of \mathbf{x} approximates the data distribution, i.e $p_\infty(\mathbf{x}) \approx p_0(\mathbf{x})$, The first term in the last equation becomes the mutual information between the internal state \mathbf{s} and the data \mathbf{x} . This leads to Eq. (8) in the main text.

B Expansion of the log-likelihood around the featureless state

In this Section we consider the expansion around the state where a_j is given by Eq. (12) and $w_{i,j} = 0$ for all i, j . For convenience, we introduce the notation $\sigma_j \equiv \sigma(a_j) = (1 + e^{-a_j})^{-1}$ which coincides with the value of \bar{x}_j in this state. A tedious calculation reveals that

$$\begin{aligned} \mathcal{L} \simeq & \sum_j \left[a_j \bar{x}_j + \log(1 - \sigma_j) + \sum_i \mathbb{E}[s_i] w_{i,j} (\bar{x}_j - \sigma_j) \right] \\ & + \frac{1}{2} \sum_{j,j'} \overline{(x_j - \sigma_j)(x_{j'} - \sigma_{j'})} \sum_{i,i'} [\mathbb{E}[s_i s_{i'}] - \mathbb{E}[s_i] \mathbb{E}[s_{i'}]] w_{i,j} w_{i',j'} \\ & - \frac{1}{2} \sum_j \sigma_j (1 - \sigma_j) \sum_{i,i'} \mathbb{E}[s_i s_{i'}] w_{i,j} w_{i',j} \\ & + \frac{1}{2} \sum_{j,j'} \left[\overline{(x_{j'} - \sigma_{j'})^2} - \sigma_{j'} (1 - \sigma_{j'}) \right] (\bar{x}_j - \sigma_j) \sum_{i,i',i''} w_{i,j'} w_{i',j'} w_{i'',j} [\mathbb{E}[s_i s_{i'} s_{i''}] - \mathbb{E}[s_{i''}] \mathbb{E}[s_i s_{i'}]] \\ & + \frac{1}{2} \sum_j (\bar{x}_j^3 + 11\sigma_j^2 - 10\sigma_j^3 - 5\sigma_j \bar{x}_j + 8\sigma_j^2 \bar{x}_j - 3\sigma_j \bar{x}_j^2 - 2\sigma_j) \sum_{i,i',i''} w_{i,j} w_{i',j} w_{i'',j} \mathbb{E}[s_i s_{i'} s_{i''}] \\ & + \sum_{j < j' < j''} \overline{(x_j - \sigma_j)(x_{j'} - \sigma_{j'})(x_{j''} - \sigma_{j''})} \sum_{i,i',i''} w_{i,j} w_{i',j'} w_{i'',j''} \mathbb{E}[s_i s_{i'} s_{i''}] \\ & - \sum_{j < j', j''} \overline{(x_j - \sigma_j)(x_{j'} - \sigma_{j'})(x_{j''} - \sigma_{j''})} \sum_{i,i',i''} w_{i,j} w_{i',j'} w_{i'',j''} \mathbb{E}[s_i s_{i'}] \mathbb{E}[s_{i''}] \end{aligned}$$

$$+\frac{1}{3} \sum_{j,j',j''} \overline{(x_j - \sigma_j)(x_{j'} - \sigma_{j'})(x_{j''} - \sigma_{j''})} \sum_{i,i',i''} w_{i,j} w_{i',j'} w_{i'',j''} \mathbb{E}[s_i] \mathbb{E}[s_{i'}] \mathbb{E}[s_{i''}]$$

Considering this expansion to second order, one finds that the featureless state is a saddle point.

B.1 Adding the first feature

We now consider the state where $w_{i,j} = 0$ for $i > 1$ and only the first feature is non-zero. For convenience we set $w_{1,j} = w_j$ and $s_1 = s$, and consider the expansion up to quadratic terms. We need to expand also with respect to a_j around the solution Eq. (12). This means that $\sigma_j = \bar{x}_j + \bar{x}_j(1 - \bar{x}_j)\delta a_j + \frac{1}{2}\bar{x}_j(1 - \bar{x}_j)(1 - 2\bar{x}_j)\delta a_j^2 + \dots$. Inserting this in the previous expression we find

$$\mathcal{L} \simeq \sum_j [\bar{x}_j \log \bar{x}_j + (1 - \bar{x}_j) \log(1 - \bar{x}_j)] \quad (29)$$

$$- \sum_j \left[\frac{1}{2} \bar{x}_j(1 - \bar{x}_j)\delta a_j^2 + \mathbb{E}[s] w_j \bar{x}_j(1 - \bar{x}_j)\delta a_j \right] \quad (30)$$

$$+ \frac{1}{2} \sum_{j,j'} w_j D_{j,j'} w_{j'} + O(w^3)$$

$$D_{j,j'} = \mathbb{E}[s] (1 - \mathbb{E}[s]) \overline{(x_j - \bar{x}_j)(x_{j'} - \bar{x}_{j'})} - \mathbb{E}[s] \bar{x}_j(1 - \bar{x}_j)\delta_{j,j'}$$

The maximisation over δa_j is done straightforwardly and

$$\delta a_j = -\mathbb{E}[s] w_j$$

inserting this into Eq. (29) leads to Eq. (13) in the main text.

B.2 Adding the next features

Let us assume that a_j and $w_{i,j}$ for $i < n$ are fixed. The gradients of the log-likelihood read

$$\frac{\partial \mathcal{L}}{\partial a_j} = \bar{x}_j - \overline{\mathbb{E}[\sigma(h_j(\mathbf{s}))|\mathbf{x}]} = 0 \quad (31)$$

$$\frac{\partial \mathcal{L}}{\partial w_{i,j}} = \overline{x_j \mathbb{E}[s_i|\mathbf{x}]} - \overline{\mathbb{E}[s_i \sigma(h_j(\mathbf{s}))|\mathbf{x}]} = 0, \quad i < n \quad (32)$$

whereas $w_{i,j} = 0$ for $i \geq n$. Here $h_j(\mathbf{s}) = a_j + \sum_{i < n} s_i w_{i,j}$ and $\mathbb{E}[\dots|\mathbf{x}]$ stand for expected values over $p(\mathbf{s}|\mathbf{x})$. Notice that s_n is independent of \mathbf{x} as long as $w_{n,j} = 0$. Let us consider the equations for $w_{n,j}$:

$$\frac{\partial \mathcal{L}}{\partial w_{n,j}} = \bar{x}_j \mathbb{E}[s_n] - \overline{\mathbb{E}[s_n \sigma(h_j(\mathbf{s}))|\mathbf{x}]} \quad (33)$$

$$= \overline{\mathbb{E}[\sigma(h_j(\mathbf{s}))|\mathbf{x}]} \mathbb{E}[s_n] - \overline{\mathbb{E}[s_n \sigma(h_j(\mathbf{s}))|\mathbf{x}]} \quad (34)$$

This is in general non-zero when $n > 1$, because s_n is not independent of $h_j(\mathbf{s})$ and hence the covariance in the last expression is non-zero. For $n = 1$ instead, $h_j(\mathbf{s}) = a_j$ is independent of \mathbf{s} and the gradients vanish, as discussed above.

C Details on the numerical experiments

For the results in Section 3.1, training is performed on NVidia V100 GPU and use 60000 training samples of each dataset, with the initial parameters \hat{w} and \mathbf{a} drawn from a Gaussian distribution with zero mean and variance 0.01.

We explored different algorithms. As discussed above, these are based on an expectation-maximisation strategy. Given that $p(\mathbf{s})$ is fixed, we first draw a sample $\hat{\mathbf{s}} = (\mathbf{s}^{(1)}, \dots, \mathbf{s}^{(N)})$ of N internal states. Then we alternate M-steps based on the usual gradient ascent with E-steps in which internal states $\mathbf{s}^{(i)}$ are assigned to data-points $\mathbf{x}^{(j)}$ in order to maximise the joint log-likelihood. In practice, an assignment coincides with a permutation $j = \pi_i$ of the integers $(1, \dots, N)$.

Algorithm A Fixed hidden probability model with assignment

Input: Training dataset \mathbf{x} , the state of hidden units \mathbf{s} is drawn from $p(\mathbf{s})$.

Initialize: $\theta^{(0)} = \{\mathbf{a}, \hat{\mathbf{w}}\}$ and the assignment $\pi = (\pi_1^{(0)}, \pi_2^{(0)}, \dots, \pi_N^{(0)})$ randomly.

Step 1: Given π , adjust the parameters θ in the direction of the gradient of log-likelihood \mathcal{L} .

Step 2: Given θ , find the best assignment π of hidden states to training data, where the matching cost function is $-\mathcal{L}$.

Repeat step 1 and 2 until convergence.

In Step 1 of Algorithm A, learning is performed in mini-batches of 20 data points and the learning rate is 0.01. In Step 2, we locate the best assignment of given hidden states to the training dataset by using the Jonker-Volgenant algorithm [35].

Algorithm B Fixed hidden probability model with bit-flip

Input: Training dataset \mathbf{x} .

Initialize: $\theta^{(0)} = \{\mathbf{a}, \hat{\mathbf{w}}\}$ randomly, and set the state of hidden units $\mathbf{s}^{(a)}$ to zero for each data point $\mathbf{x}^{(a)}$.

Step 1: Fixed \mathbf{s} , adjust the parameters θ in the direction of the gradient of log-likelihood \mathcal{L} .

Step 2: Flip one bit of \mathbf{s} for each data point and accept the change if \mathcal{L} increases.

Repeat step 1 and 2 until convergence.

In Step 2 of Algorithm B, we explore different prescriptions of how to chose the spin to flip. Results do not change considerably. Note that the resolution $H[\mathbf{s}]$ increases during training. It starts from $H[\mathbf{s}] = 0$ and then slowly raises to its maximum, as shown in figure

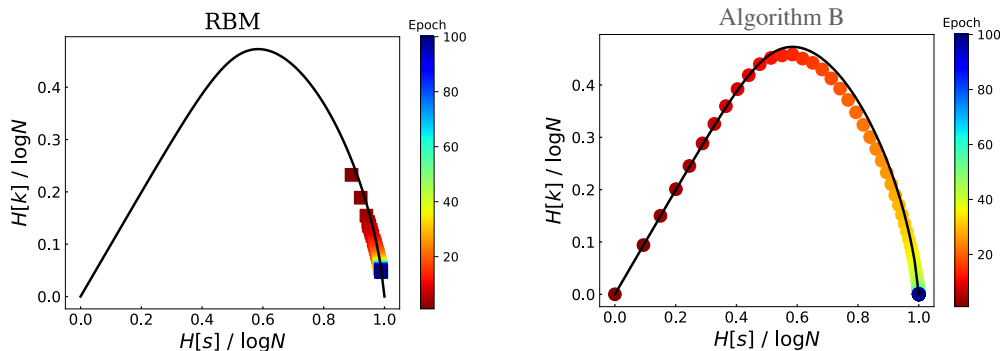


Figure 10: The relevance $H[k]$ as a function of the resolution $H[s]$ of the hidden states for an RBM with CD1 algorithm (left) and Algorithm B with $p(s) = 2^{-n}$ (right). Both models are trained for 100 epochs on the MNIST dataset. The full black curve is the theoretical maximum of $H[k]$.

10. By contrast, in the RBM $H[s]$ starts at its maximal value and then decreases. Both in our model and in the RBM, the relevance $H[k]$ stays close to its theoretical maximum [5], suggesting that both models extract the maximal information from the data [4].

Let us now come to the results of Section 3.2. We train the model incrementally adding one feature at a time. The algorithm we use, for each number n of internal nodes, is similar to Algorithm B above, we use Algorithm B with two important differences:

a) The initial weights are not random. The addition of the n^{th} feature to the trained model $p(\mathbf{x}, \mathbf{s} | \hat{\theta}_{n-1})$ with $n - 1$ features, entails enlarging the state space with the addition of feature s_n . Yet the gradients with respect to $w_{n,j}$ remain zero unless the new feature is "switched on" for some data point $\mathbf{x}^{(i)}$, i.e. $s_n^{(i)} = 1$. The HFM predicts the number

$$N_n^{(0)} = N \sum_{s_1=0}^1 \dots \sum_{s_{n-1}=0}^1 p(s_1, \dots, s_{n-1}, 1)$$

of data points that should have $s_n = 1$. We initially set $s_n = 1$ for the $N_n^{(0)}$ points $\mathbf{x}^{(i)}$ with the lowest joint log-likelihood. This in turn allows us to compute an initial value of the n^{th} feature \vec{w}_n , as the one that maximises the likelihood, when the internal states and all other features (i.e the parameters $\hat{\theta}_{n-1}$) are kept fixed. This is the starting point of the EM algorithm, which alternates E-steps and M-steps.

b) In the E-step we set

$$\mathbf{s}^{(i)} = \arg \max_{\mathbf{s}} \log p(\mathbf{x}^{(i)}, \mathbf{s} | \theta_n)$$

for all data points, where θ_n is the current value of the parameters. In the M-steps we perform gradient ascent on the log-likelihood (we execute $n_g = 5$ gradient ascent steps

by line search with Armijo rule). We alternate E- and M-steps until no data point $\mathbf{x}^{(i)}$ is reassigned to a different internal state $\mathbf{s}^{(i)}$.